

[¹¹C]Glycylsarcosine: synthesis and in vivo evaluation as a PET tracer of PepT2 transporter function in kidney of *PepT2* null and wild-type mice[☆]

Nabeel B. Nabulsi,^a David E. Smith^b and Michael R. Kilbourn^{a,*}

^a*Division of Nuclear Medicine, Department of Radiology, School of Medicine, The University of Michigan, Ann Arbor, MI 48109, USA*

^b*Department of Pharmaceutical Sciences, College of Pharmacy, The University of Michigan, Ann Arbor, MI 48109, USA*

Received 26 October 2004; revised 1 February 2005; accepted 1 February 2005

Abstract—[¹¹C]Glycylsarcosine (Gly-Sar) was synthesized as a potential radiotracer to investigate the localization and in vivo function of the peptide transporter PepT2 in mouse kidney. Its C-11 labeled diketopiperazine derivative, [¹¹C]cyclo(Gly-Sar) [1-methylpiperazine-2,5-dione], was also evaluated as a potential tracer. [¹¹C]Gly-Sar exhibited rapid initial uptake into kidneys with slow clearance from the medulla, consistent with uptake and retention of the radiotracer through the actions of PepT2. In contrast, the corresponding cyclized dipeptide [¹¹C]cyclo(Gly-Sar) showed rapid clearance and accumulation only in the renal pelvis region. Involvement of *PepT2* in reabsorption and delayed clearance of [¹¹C]Gly-Sar was confirmed using the *PepT2* knockout mouse, where rapid renal elimination of [¹¹C]Gly-Sar and the absence of radioactivity in medulla were observed. This study demonstrates using in vivo imaging technique that *PepT2* is primarily responsible for renal tubular active reabsorption of Gly-Sar, and provides a new tool for studying tubular peptide reabsorption and clearance.

© 2005 Elsevier Ltd. All rights reserved.

1. Introduction

The peptide transporters PepT1 and PepT2 actively transport di- and tripeptides including peptidomimetics across cell membranes in animals, microbes and plants.^{1–3} Their capacity to transport a large variety of drugs, including angiotensin-converting enzyme inhibitors, β -lactam antibiotics and the anti-cancer drug bestatin (for reviews, see Refs. 3–5) exemplify their pharmacological importance. PepT1 is a low-affinity/high-capacity transporter, which is found primarily on the brush-border membrane of the small intestine, and to a lesser extent in the proximal tubule of the kidney.^{6,7} PepT2 is a high-affinity/low-capacity transporter expressed predominantly in the apical membrane of

kidney,^{6,7} but which has also been identified in the lung, brain, and mammary gland.^{8–11} Both transporters function electrogenically, as they are driven electrochemically via a gradient of protons across the intestinal or renal brush-border membrane in the lumen-to-cytoplasm direction.¹² In addition to amino acid transporters, peptide transporters contribute to the homeostasis of amino acids.¹³

Expression of *PepT2*, and to a lesser extent *PepT1*, in kidney has raised questions regarding their overall physiological contribution in tubular reabsorption. Whereas *PepT1* was found in segment S1 of the proximal tubule, *PepT2* was localized in segments S2 and S3,⁶ thus allowing conservation of peptide-bound amino acids through maximizing reabsorption. In the rat, using radiolabeled molecular probes and RT-PCR, *PepT1*-mRNA was assigned to the cortex region, while *PepT2*-mRNA was assigned to the outer stripe of the outer medulla.⁷ The significance of *PepT2* vis-à-vis peptide uptake in kidney,¹⁴ in addition to the choroid plexus,¹⁵ was recently demonstrated in targeted disrupted *PepT2* gene in mice. Both studies reported markedly reduced uptake of *PepT2*-substrate peptides.

Keywords: [¹¹C]Glycylsarcosine; Gly-Sar; Renal uptake; *PepT1* and *PepT2* peptide transporters.

[☆]Presented in part at the 51st annual meeting of the Society of Nuclear Medicine, Philadelphia, PA, June 19–23, 2004; *J. Nuc. Med.* **2004**, *45* (5) supp., 443p, abstract no. 1380.

*Corresponding author. Tel.: +1 734 763 9246; fax: +1 734 764 0288; e-mail: mkilbour@umich.edu

Understanding renal reabsorption and carrier-mediated transport in the small intestine are important issues in drug delivery and performance. Accurate knowledge of renal drug clearance mechanisms can be vital for certain populations, especially when the kidney function is compromised.^{16,17} When drug toxicity is an issue, knowledge of excretory pathway in the kidney can be beneficial for tailoring individualized drug therapy: for example, tubular reabsorption of cephalosporins and penicillin antibiotics is offset by their secretion into the tubular lumen.¹⁸ Both PepT1 and PepT2 may play a role in the pharmacokinetics of β -lactam antibiotics by transporting them into target cells and promote reabsorption into renal tubular cells after glomerular filtration.³

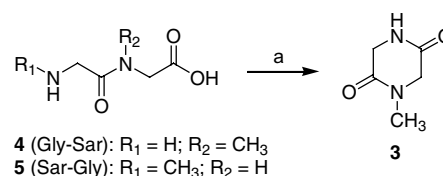
In view of the pharmacological importance of peptide transporters, we have synthesized Gly-Sar labeled with the positron-emitting radionuclide carbon-11 ($t_{1/2} = 20.4$ min) as a potential radiotracer for functional imaging of PepT2 in kidney. Gly-Sar is a hydrolysis-resistant dipeptide that is frequently used as a model substrate for PepT1 and PepT2.^{19,20} To date, however, [¹¹C]Gly-Sar has not been synthesized. We also examined [¹¹C]-*cyclo*(Gly-Sar), its diketopiperazine derivative, as a potential PET tracer. Transport of cyclic dipeptides by PepT1 and PepT2 has been controversial.^{21–23} Our results using *PepT2* knockout mice unequivocally demonstrate that PepT2 is the peptide carrier primarily responsible for the active renal tubular reabsorption of [¹¹C]Gly-Sar, but the [¹¹C]*cyclo*(Gly-Sar) analog was not recognized by PepT2. [¹¹C]Gly-Sar could have potential for indirectly probing the pharmacokinetics of drugs as a function of renal tubular reabsorption, thus providing biodistribution data in the same animal over time. Traditionally, pharmacokinetic and pharmacodynamic studies are obtained in humans from the concentration of drug in blood or other body fluid.²⁴

2. Results and discussion

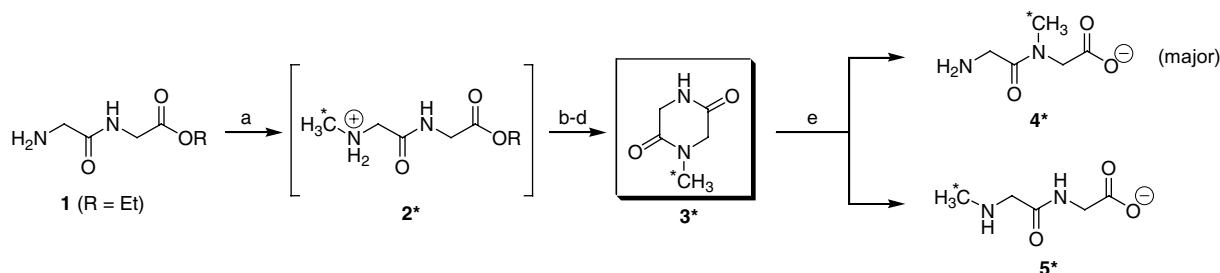
Nonradioactive Gly-Sar **4** is commercially available. An important issue in choosing a synthetic approach for preparing the radiolabeled ligand was the ability to separate Gly-Gly (glycylglycine) from Gly-Sar. Gly-Gly impedes the uptake of Gly-Sar by PepT2, with apparent K_i values of 0.091 ± 0.005 (Gly-Gly) and 0.372 ± 0.017 (Gly-Sar) mM.²⁵ Scheme 1 outlines our synthetic approach to radiolabeled Gly-Sar **4***. The first phase

involved preparation of the requisite diketopiperazine intermediate [¹¹C]*cyclo*(Gly-Sar) **3***. This was synthesized via intramolecular aminolysis of the ethyl ester derivative [¹¹C]Sar-Gly-OEt **2***, which was prepared in situ from commercially available precursor glycylglycinate **1**. The standard sample of *cyclo*(Gly-Sar) **3** was prepared via intramolecular aminolysis of either Gly-Sar **4** or Sar-Gly **5** according to known procedures (Scheme 2). Therefore reaction of **1** with [¹¹C]methyl triflate yielded radiolabeled **2***, which subsequently underwent facile intramolecular aminolysis to the diketopiperazine (DKP) derivative **3*** in 6–13% radiochemical yield (decay corrected) upon heating in an aqueous solution of ammonium acetate (25–50 mmol) for 5 min at 80 °C and in the presence of triethyl amine. As revealed by HPLC, intramolecular aminolysis proceeded smoothly with total conversion of **2*** and excess starting material **1** to their corresponding diketopiperazines, the [¹¹C]*cyclo*(Gly-Sar) **3*** ([¹¹C]1-methylpiperazine-2,5-dione or 1-methyl-2,5-diketopiperazine) and glycine anhydride (piperazine-2,5-dione or 2,5-diketopiperazine), respectively. Small volume of DMSO was added to the reaction mixture only to prevent possible charring while evaporating acetonitrile. Its effect on the course of the reaction was not investigated. However larger volumes of polar solvents prevented separation of **3*** by causing early elution with the solvent front.

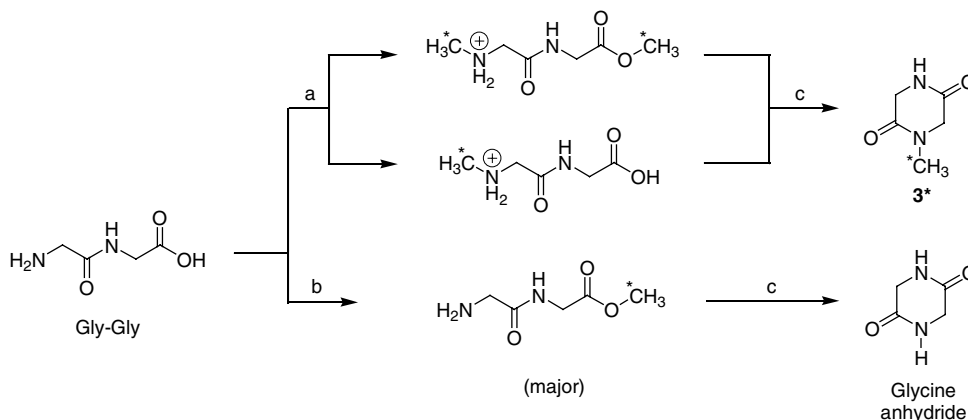
Gly-Gly-OH was used as precursor early in the developmental stages to prepare **3*** (Scheme 3). Lower radiochemical yields were obtained from the reaction with [¹¹C]methyl iodide at ambient temperature followed by refluxing in DMF or DMSO for 20–30 min. With [¹¹C]methyl triflate, small amount of **3*** was detected. Apparently methylation of the carboxylate predominates from reaction with the more reactive CH_3^+ carbocation of [¹¹C]methyl triflate. At room temperature, [¹¹C]methyl triflate reacted with Gly-Gly and yielded mainly one product, with retention time comparable to



Scheme 2. Reagents and conditions: (a) glycol, 195 °C, 48–70%.



Scheme 1. Reagents and conditions: (a) [¹¹C]CH₃OTf, MeCN/DMSO, -40 °C; (b) evaporate MeCN; (c) Et₃N/25 mmol NH₄OAc, 80 °C, 5 min; (d) HPLC; (e) 2N NaOH, 100 °C, 8 min.



Scheme 3. Reagents and conditions: (a) $[^{11}\text{C}]\text{CH}_3\text{I}$, DMF or DMSO, 24 °C; (b) $[^{11}\text{C}]\text{CH}_3\text{OTf}$, DMF or DMSO, 24 °C; (c) 150–195 °C, 20–30 min.

ethyl glycylglycinate. Albeit, intramolecular aminolysis of the resulting methyl ester is unproductive because, as exemplified in Scheme 3, it can only yield the glycine anhydride derivative.

Effect of pH, temperature, buffer concentration, and buffer species on diketopiperazine formation was studied in detail.²⁶ We found the use of triethylamine essential for intramolecular aminolysis of **2***, and only a small amount of *cyclo*(Gly-Sar) **3*** was detected in the absence of the catalyst. Without the catalyst, aminolysis did not occur in refluxing acetonitrile, while 3–4% radiochemical yields of **3*** were obtained by refluxing **2*** in DMF or DMSO for prolonged periods, generally 20–30 min. The importance of amines and alkyl ammonium carboxylates on intramolecular aminolysis of dipeptides have been described.^{27,28} It is unclear whether facile for-

mation of *cyclo*(Gly-Sar) **3*** was due to a sort of synergistic catalysis between triethylamine and ammonium acetate.

The second phase in the synthesis involved basic hydrolysis of the isolated $[^{11}\text{C}]\text{cyclo}(\text{Gly-Sar})$ **3***. Refluxing **3*** in aqueous NaOH proceeded with a >99.5% conversion to the corresponding linear dipeptide(s). The mechanism for ring-opening of *cyclo*(Gly-Sar) **3**, including other diketopiperazines, was previously studied in detail and was reported to yield a mixture of the isomers Gly-Sar **4** and Sar-Gly **5** in a ratio 3.4 to 1.²⁷ Figure 1 illustrates the HPLC radioactivity chromatogram for the hydrolysis reaction and chromatograms of the standards Gly-Sar **4**, Sar-Gly **5**, and *cyclo*(Gly-Sar) **3**. The hydrolysis yielded primarily Gly-Sar **4**. The exact composition could not be determined because it was not possible to

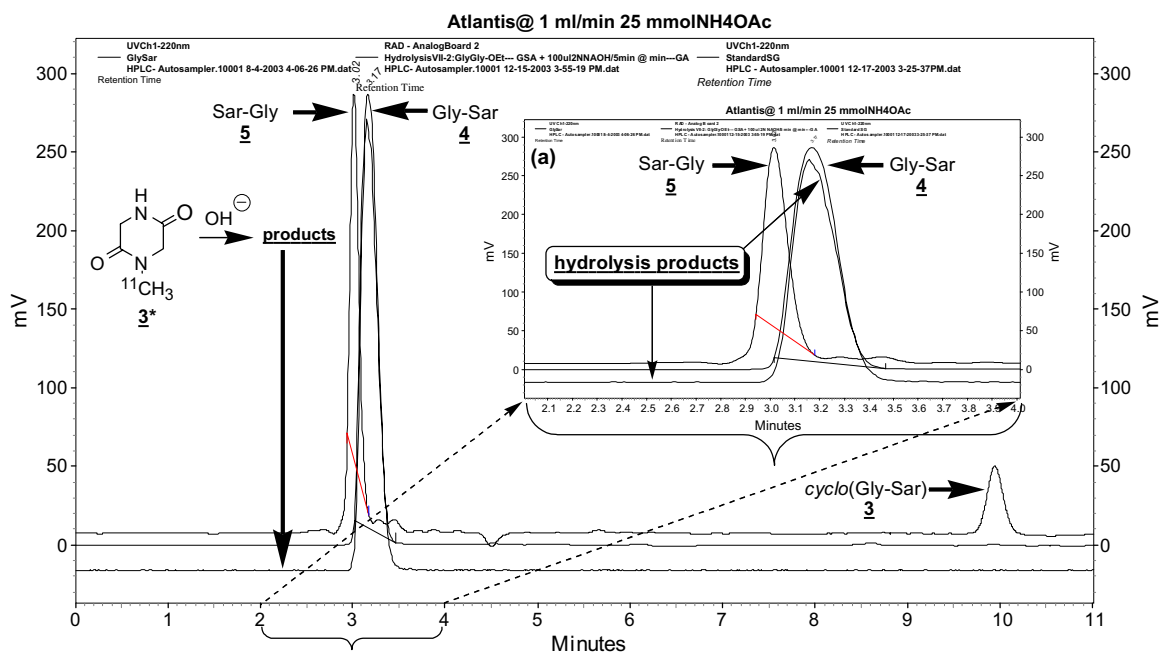
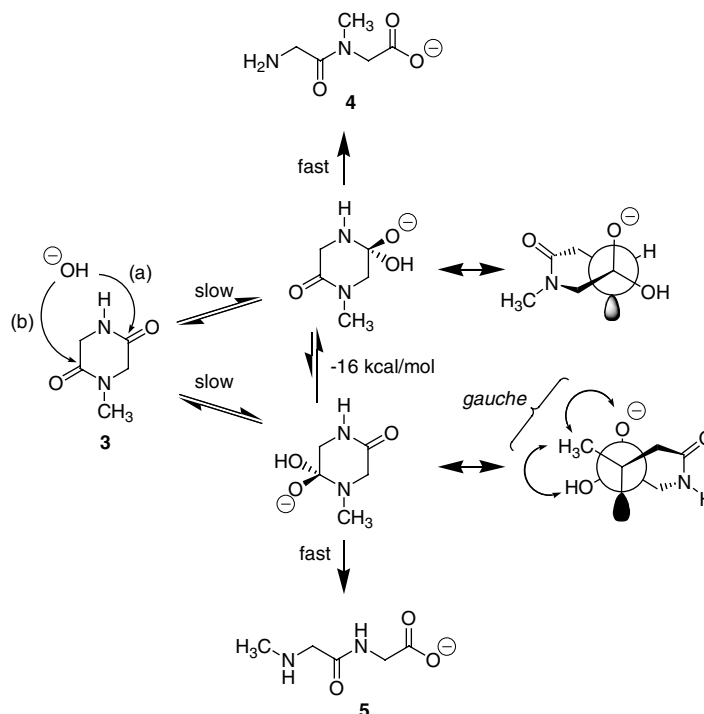


Figure 1. Reverse-phase HPLC profile for hydrolysis of $[^{11}\text{C}]\text{cyclo}(\text{Gly-Sar})$ **3*** (radioactivity chromatogram bottom dotted line) superimposed over HPLC profile of the standard Gly-Sar **4** co-injected with mixture of Sar-Gly **5** and *cyclo*(Gly-Sar) **3** standards. (Inset **a** shows expansion of the region in between 2 and 4 min.) Mobile phase used for both QC analysis and standards (25 mmol aqueous ammonium acetate) were identical.



Scheme 4. MMFF94s calculations of tetrahedral structures resulting from addition of hydroxide ion to the carbonyl carbon. Related Newman projections illustrate absence and/or presence of unfavorable gauche interactions.

obtain base-line separation between Gly-Sar **4** and Sar-Gly **5** with our HPLC system. Careful review of the hydrolysis mechanism clarifies why formation of Gly-Sar **4** predominates (Scheme 4). Addition of the hydroxide ion to *cyclo*(Gly-Sar) **3** is rate controlling.²⁹ Our MMFF94^{30–33} molecular mechanics calculations indicate that the tetrahedral structure resulting from addition of the hydroxyl to the carbonyl of the secondary amide leading to formation of Gly-Sar **4**, route a, is more favorable by 16 kcal/mol.³⁴ Route b, forming the tetrahedral intermediate leading to Sar-Gly **5** is accompanied by two unfavorable *gauche* interactions between the *N*-methyl group and the vicinal oxygens of C₂. These results are in accord with the published kinetic study,²⁷ which showed formation of Gly-Sar **4** is favored by 3.4 over Sar-Gly **5**.

Ex vivo biodistribution studies were carried out with normal CD-1 mice. Figures 2 and 3 illustrate biodistribution in the blood, liver, lung, and spleen. In general, [¹¹C]*cyclo*(Gly-Sar) **3*** uptake was slightly higher than [¹¹C]Gly-Sar **4***. [¹¹C]*cyclo*(Gly-Sar) **3*** exhibited analogous uptake and clearance in the blood, liver, lung, and spleen. Brain uptake was very small for both **4*** and **3***. On the other hand, uptake of [¹¹C]Gly-Sar **4*** appeared higher in the spleen relative to the blood, lung, and liver, with least uptake in the liver.

Biodistribution curves were also obtained for [¹¹C]Gly-Sar **4*** and [¹¹C]*cyclo*(Gly-Sar) **3*** in kidney (see Fig. 5b). The resulting data are quite similar to that obtained from the in vivo time-activity study (Fig. 5a). The initial renal uptake of **4*** was clearly about three times larger than **3***. The higher uptake and slow clearance of

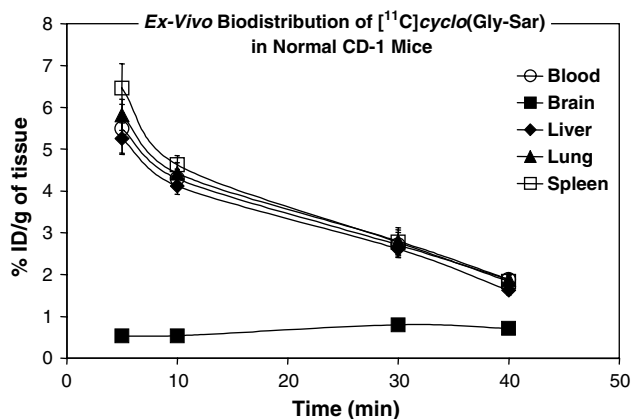


Figure 2. Ex vivo biodistribution (%ID/g of tissue) for [¹¹C]*cyclo*(Gly-Sar) **3*** in blood (○), brain (■), liver (◆), lung (▲) and spleen (□) for CD-1 mice (*n* = 4, shown as mean ± SD).

[¹¹C]Gly-Sar **4*** suggests involvement of an active transport mode.

In vivo studies were also conducted with CD-1 and *PepT2* knockout mice. Figure 4a–d illustrates microPET images of CD-1 mouse kidneys, obtained with microPET R4 following 2–10 min post-injection of both [¹¹C]Gly-Sar **4*** and [¹¹C]*cyclo*(Gly-Sar) **3*** (images obtained with microPET P4 are not shown). Accumulation of [¹¹C]Gly-Sar **4*** is remarkable in the medulla (outer medulla) region, where *PepT2*-mRNA is known to be expressed.^{7,8} On the other hand, [¹¹C]*cyclo*(Gly-Sar) **3*** is largely visible through the renal pelvis region, most likely resulting from its rapid excretion. Figure 5a shows

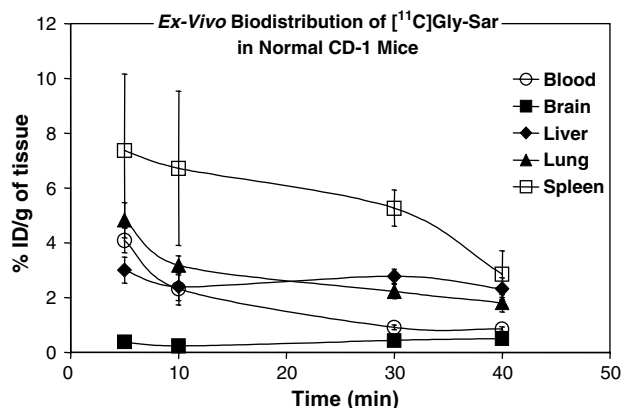


Figure 3. Ex vivo biodistribution (%ID/g of tissue) for $[^{11}\text{C}]\text{Gly-Sar } 4^*$ in blood (\circ), brain (\blacksquare), liver (\blacklozenge), lung (\blacktriangle), and spleen (\square) for CD-1 mice ($n = 4$, shown as mean \pm SD).

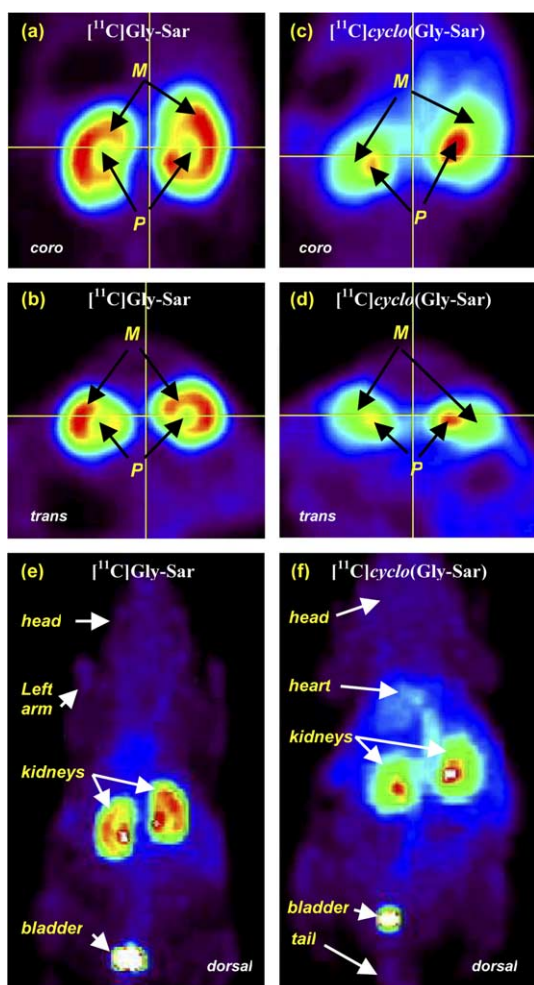
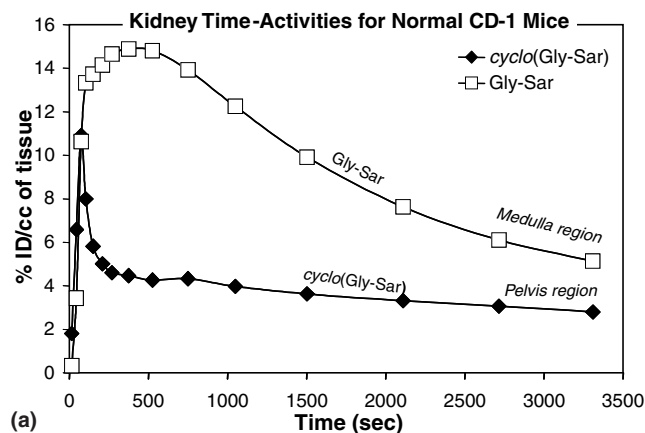
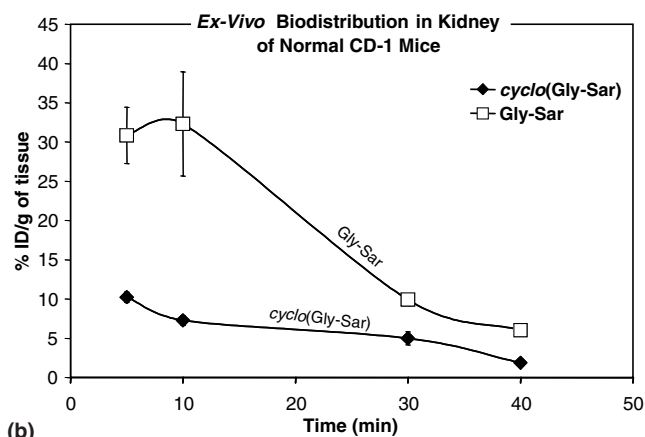


Figure 4. MicroPET images of CD-1 mice—coronal (a) and transverse and (b) images of kidneys showing uptake of $[^{11}\text{C}]\text{Gly-Sar } 4^*$ in medulla (M), 10 min post-injection; coronal (c) and transverse and (d) images 2 min post-injection of $[^{11}\text{C}]\text{cyclo(Gly-Sar) } 3^*$ with radioactivity visible through the renal pelvis (P) region; (e) and (f) depict uptake of $[^{11}\text{C}]\text{Gly-Sar } 4^*$ and $[^{11}\text{C}]\text{cyclo(Gly-Sar) } 3^*$ in kidneys with respect to the whole mouse (time frames different than for a–d).

related time-activity curves for the corresponding regions of interest (data from microPET P4 are not



(a)



(b)

Figure 5. (a) Time-activity curves (%ID/cc of tissue) for $n = 1$ depicting slow renal clearance of $[^{11}\text{C}]\text{Gly-Sar } 4^*$ (\square ; ROI = right Medulla; ID = 1.7 mCi) versus $[^{11}\text{C}]\text{cyclo(Gly-Sar) } 3^*$ (\blacklozenge ; ROI = right Pelvis; ID = 3.0 mCi) in CD-1 mice; (b) ex vivo biodistribution (%ID/g of tissue) of $[^{11}\text{C}]\text{Gly-Sar } 4^*$ (\square) and $[^{11}\text{C}]\text{cyclo(Gly-Sar) } 3^*$ (\blacklozenge) in kidney of normal CD-1 mice ($n = 4$, shown as mean \pm SD); Both the dissection and imaging methods gave essentially similar results.

shown), revealing fast initial kidney uptake for both $[^{11}\text{C}]\text{Gly-Sar } 4^*$ and $[^{11}\text{C}]\text{cyclo(Gly-Sar) } 3^*$. However, and in agreement with the ex vivo biodistribution data (Fig. 5b), $[^{11}\text{C}]\text{Gly-Sar } 4^*$ uptake was greater than its cyclic derivative 3^* , and radioactivity clears more gradually. These results suggest that only $[^{11}\text{C}]\text{Gly-Sar } 4^*$ is transported by PepT2. That $[^{11}\text{C}]\text{cyclo(Gly-Sar) } 3^*$ is not recognized by PepT2 is concluded from exclusion of radioactivity from the medulla region and from the profile of the corresponding time-activity curves.

As pointed out above, we also imaged a $\text{PepT2}^{-/-}$ mouse to verify the above observations regarding transport dynamics of $[^{11}\text{C}]\text{Gly-Sar } 4^*$. These transgenic mice are similar to those employed in previous studies and were without obvious behavioral or neurological abnormalities.^{14,15} They exhibited normal urine protein levels and comparable base-line blood chemistries. Gross and light microscopic morphology of the kidneys of the null mouse were normal.¹⁵ PepT1 transporter was retained in the kidney,¹⁵ and was shown to function normally by imaging with the fluorophore-conjugated dipeptide substrate D-Ala-Lys-AMCA.¹⁴

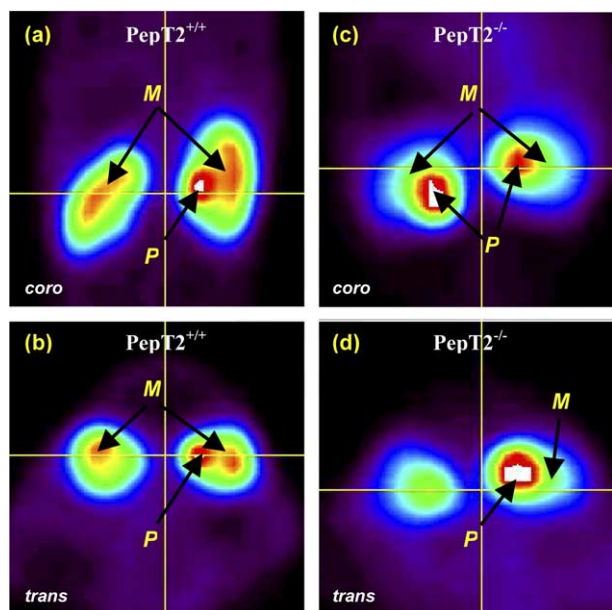


Figure 6. MicroPET images for kidney uptake of [^{11}C]Gly-Sar **4*** in transgenic mice—coronal (a) and transverse (b) images of *PepT2*^{+/+} mouse, 15 min post-injection, with radioactivity visible through the medulla (M) and pelvis (P) regions; coronal (a) and transverse (b) images of *PepT2*^{-/-} mouse, 1.5 min post-injection, with radioactivity visible in only the pelvis region.

Figure 6 depicts microPET images for the null (*PepT2*^{-/-}) and wild type (*PepT2*^{+/+}) mice following 1½ and 15 min post-injection. The time-activity profile for the transport of [^{11}C]Gly-Sar **4*** in the kidney of the *PepT2*^{+/+} mouse was similar to that observed in the normal CD-1 mice, but with radioactivity visible in both the renal medulla and the pelvis regions. It is unclear why radioactivity is more pronounced in the pelvis region of the *PepT2*^{+/+} mouse relative to the CD-1 type even when compared at the same time frame. As mentioned above, these mice showed no obvious abnormalities, except that they are significantly smaller than the CD-1, and in particular the *PepT2*^{+/+} mouse was 3 g lighter than the average CD-1.

As expected, the *PepT2*^{-/-} mouse distinctly lacked accumulation of [^{11}C]Gly-Sar **4*** in the medulla region owing to the absence of PepT2. The corresponding time-activity curves (Fig. 7) shows faster clearance from the medulla region for the *PepT2*^{-/-} mouse. Furthermore, diminished (or lack of) tubular reabsorption in this region is also suggested by faster time-to-peak period relative to the wild type (Fig. 7), while both *PepT2*^{-/-} and *PepT2*^{+/+} exhibited similar pelvic time-to-peak period (Fig. 8).

3. Conclusions

We have synthesized C-11 labeled Gly-Sar, the frequently used model substrate for PepT1 and PepT2, as a potential PET tracer. With the combined use of *PepT2*^{-/-} knockout mouse, we examined the functional role of PepT2 in the renal transport of dipeptides in vivo.

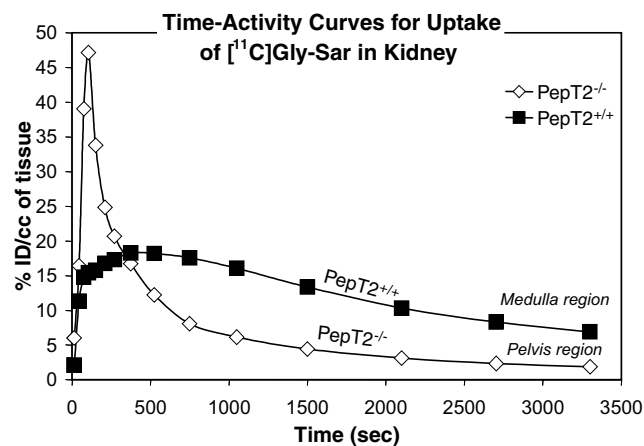


Figure 7. Time-activity curves (%ID/cc of tissue) for $n = 1$ reflecting renal uptake of [^{11}C]Gly-Sar **4*** in right kidneys of transgenic mice; the *PepT2*^{-/-} (\diamond ; ROI = Pelvis; ID = 1.4 mCi, measured with P4) and *PepT2*^{+/+} (\blacksquare ; ROI = Medulla; ID = 1.0 mCi).

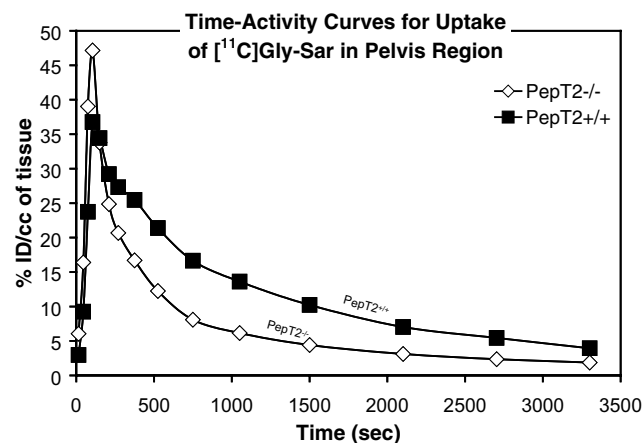


Figure 8. Time-activity curves (%ID/cc of tissue) for $n = 1$ reflecting renal uptake of [^{11}C]Gly-Sar **4*** in pelvis regions of transgenic mice; the *PepT2*^{-/-} (\diamond , ID = 1.4 mCi, measured with P4) and *PepT2*^{+/+} (\blacksquare , ID = 1.0 mCi).

There was an obvious deficiency in the renal uptake of [^{11}C]Gly-Sar in the *PepT2*^{-/-} mouse. Furthermore, exclusion of [^{11}C]Gly-Sar **4*** activity from the renal medulla (outer medulla) region of the *PepT2*^{-/-} mouse, where PepT2-mRNA is expressed, suggests that PepT2 is primarily responsible for the renal tubular active reabsorption of Gly-Sar, and perhaps similar substrates that utilize the same transport pathway such as di- and tripeptides, β -lactam antibiotics of the cephalosporin and penicillin class, and the anticancer agent bestatin. Finally, the cyclic dipeptide analog, [^{11}C]cyclo(Gly-Sar), was not transported by PepT2.

4. Experimental section

4.1. Materials and methods

Thin layer chromatography (TLC) was performed on precoated 60F-254 silica gel plates (E. Merck). ^1H and

^{13}C NMR spectra were recorded on Bruker DPX-300 MHz spectrometer. Electron ionization, chemical ionization, and high resolution mass spectra were performed on a V. G. Analytical 70–250S spectrometer (Micromass, Manchester, UK). HPLC analyses were performed with a Shimadzu VP series. Radioactivity detection was done with Bioscan coincidence (model B-FC-4000) detector. UV detection was performed at 220 nm ($\text{C}=\text{O}$ $\lambda_{\text{max}} \sim 170\text{--}210$ nm) with minor baseline noise because mobile phase contains no organics besides ammonium acetate buffer (UV cutoff = 205 nm³⁵) and phosphate buffer (UV cutoff = 190 nm³⁵). Melting points were determined on a Mel-Temp apparatus (Laboratory Devices, Cambridge, MA) and are uncorrected. Sar-Gly (sarcosylglycine) was purchased from Bachem Bioscience Inc., King of Prussia, PA. All other reagents and solvents were purchased from Aldrich Chemical (Milwaukee, WI) or Fisher Scientific (Pittsburgh, PA) and were used without further purification unless noted. Radiochemical yields and duration of syntheses are reported as decay corrected to the end of cyclotron target bombardment.

Animal experiments were carried out according to the University of Michigan Committee on Use and Care of Animals (UCUCA). Biodistribution studies with normal CD-1 mice (Charles Rivers, Wilmington, MA, USA) were done in females weighing 20–25, 26 and 27 g for microPET imaging. The *PepT2*^{-/-} and *PepT2*^{+/+} mice weighed 20 and 24 g, respectively, and were as described elsewhere.^{14,15}

4.1.1. 1-Methyl-2,5-piperazinedione (3). Modifying literature method,³⁶ a solution of glycylsarcosine **4** (3 g, 0.0205 mol) in 18 mL anhydrous ethylene glycol was refluxed for 3 h. The solvent was evaporated under vacuo. The resulting greenish solid was recrystallized from isopropanol to give 1.26 g (48%) of **3** as light greenish solid with mp 140–142 °C (lit: 141–143 °C;³⁶ 142–143 °C;³⁷ 136–139 °C;³⁸ 135.5–139 °C³⁹). The filtrate was diluted with isopropyl ether and allowed to stand for several days. Slow evaporation of the solvent yielded 0.58 g additional **3** as colorless to light green plates for a total yield of 70%. ^1H NMR (DMSO-*d*₆) δ 2.81 ppm (s, 3H, >N-CH₃), 3.77 (s, 2H, -CH₂-), 3.88 (s, 2H, -CH₂-), 8.11 (s, 1H, >N-H); ^{13}C NMR (DMSO-*d*₆) δ 32.8 ppm, 44.3, 51.1, 164.0, 165.4. EIMS *m/z* (relative intensity): 128 [100, M⁺]. HRMS (EI) calculated for C₅H₈N₂O₂ (M⁺) 128.0586, found 128.0589. HPLC, 220 nm; (a) Waters C-18, *Atlantis* (4.6 × 250 mm), 50 mmol aq NH₄OAc, *t*_R = 6.5 min at a flow rate of 1.5 mL/min; *t*_R = 10 min at 1 mL/min; (b) Showa Denko polymethacrylate, RSpak *Shodex* DE-613 (6.0 × 150 mm), 50 mmol aq NH₄OAc, *t*_R = 5.1 min at 1.0 mL/min.

4.1.2. [^{11}C]cyclo(Glycylsarcosine) (3*). No-carrier-added [^{11}C]CO₂ was prepared by proton bombardment of nitrogen gas target [$^{14}\text{N}(p,\alpha)^{11}\text{C}$], which was converted to [^{11}C]methyl iodide according to the conventional lithium aluminum hydride (LAH) reduction/hydroiodic acid (HI) method, then converted to [^{11}C]methyl triflate successively.⁴⁰ About 5–10 min before end of beam,

1 mL of anhydrous acetonitrile was added to a vial containing 10 mg of glycylglycine ethyl ester hydrochloride **1**-HCl, followed by 1 equiv (~7.1 μL) of triethylamine, and the resulting mixture was vortex-mixed until total dissolution. Then 150 μL of the resulting solution was transferred into a 1000 μL reaction vial containing 10 μL of anhydrous DMSO. [^{11}C]Methyl triflate was distilled into the reaction solution at about -40 °C⁴¹ in N₂ carrier (30 mL/min) until radioactivity had peaked. The resulting mixture was heated at 170 °C for 1 min allowing acetonitrile to evaporate through a vent line. N₂ gas was passed through the reaction vial in order to sweep away acetonitrile vapors, and then cooled to about 50 °C while sweeping through N₂. A mixture of 25 μL triethylamine in 400 μL aqueous solution of 25 mmol of ammonium acetate was added to the reaction vial, and the resulting solution was heated at 80 °C for 5 min. After cooling to ambient temperature, the mixture was injected onto Waters *Atlantis* C-18 (4.6 × 250 mm) analytical HPLC column eluting with 25 mmol ammonium acetate at 1.5 mL/min at 220 nm. [^{11}C]cyclo(Gly-Sar) **3*** eluted at 6.5 min⁴² and collected into a sterile vial. The resulting radiochemical yield was 5.9% (*n* = 2) with >99.5% radiochemical purity determined by injection onto either the *Atlantis* column or the *Shodex*. Total synthesis time was 34 min. For animal studies, the labeled compound was used directly with CD-1 mice without further formulation.

4.1.3. [^{11}C](Glycylsarcosine) (4*). The [^{11}C]cyclo(Gly-Sar) **3*** intermediate, prepared as described above, was collected upon HPLC purification into a sterile vial containing 120 μL of 2 N NaOH and the mixture was refluxed for 8 min.⁴³ The resulting solution was cooled, and excess hydroxide was neutralized with 250 μL NaH₂PO₄ buffer. The average radiochemical yield was 8.6% (5.3–13.1%, *n* = 8), with specific activity of 1395 mCi/ μmol , and >99.5% radiochemical purity determined by injecting onto the *Atlantis* column at 1 mL/min (*t*_R = 3.2 min). No additional formulation was required for animal studies with CD-1 mice. On the other hand, the solution was first filtered through 0.22 μm sterile filter and diluted with sterile water before injecting into the knockout mouse. Total synthesis time was about 42 min.

4.2. MicroPET imaging

MicroPET R4 and microPET P4 positron emission tomography instruments (Concorde Microsystem Inc., Knoxville, TN) were used for imaging. Higher doses (+50%) are used when employing the P4 instrument in order to offset its 30% lower sensitivity. This should not affect data interpretation, since resolution is similar with both instruments and their images are processed by similar protocol.

Animals were anesthetized with isoflurane and placed on the bed of the instrument. Animals were then injected as a bolus via an indwelling tail vein catheter with 1–3 mCi of radiotracer and imaged for 60 min. Data were acquired in list mode for 60 min, and then temporally binned into a series of variable frame lengths; (i)

for [^{11}C]Gly-Sar and [^{11}C]cyclo(Gly-Sar) in CD-1 mice: 12 frames each; $5 \times 2 \text{ min} + 4 \times 5 + 3 \times 10$; (ii) for [^{11}C]Gly-Sar in *PepT2* mice: 15 frames each; $4 \times 0.5 \text{ min} + 3 \times 1 + 2 \times 2.5 + 2 \times 5 + 4 \times 10$. A model-based normalization⁴⁴ specific to the microPET scanner geometry and block design was applied to the sonogram data. Data were also corrected for random coincidences, dead time, attenuation, and scatter. Images were reconstructed using fully 3-D maximum a-posteriori (MAP) 30 iterations.⁴⁵ Regions of interest (ROI) corresponding to the renal medulla and pelvis were drawn manually on multiple slices (i.e., 3-D) of specified frame of each dynamic sequence and applied to all other frames generating time-activity curves: (i) CD-1 mice: for [^{11}C]cyclo(Gly-Sar), frame 0 (2 min post-injection); for [^{11}C]Gly-Sar, frame 4 (10 min post-injection); (ii) *PepT2*^{-/-} mouse: for [^{11}C]Gly-Sar, frame 2 (1.5 min post-injection); (iii) *PepT2*^{+/+} mouse: for [^{11}C]Gly-Sar, frame 9 (15 min post-injection).

4.3. Ex vivo biodistribution studies

Groups of mice (four animals) were anesthetized with diethyl ether and injected via the tail vein with a saline diluted solution of radiotracer (20–300 μCi in 25 mmol NH_4OAc). Animals were allowed to recover, reanesthetized and sacrificed at 5, 10, 30 or 40 min post-injection. The organs were rapidly removed, weighed and then counted for carbon-11 using an automatic gamma counter (Packard Auto Gamma 5780). Counts were decay corrected to the time of injection to determine the percent injected dose per gram tissue (%ID/g) for each organ.

Acknowledgements

This study supported by grants from Department of Energy (DE-FG02-87ER60561) and National Institutes of Health (T-32-CA009015; R01 GM035498). We are thankful for Mr. Phillip Sherman for performing the biodistribution studies and preparing animals for microPET imaging. We also thank Mr. James Moskwa for carrying out and reconstructing the microPET images. We extend our gratitude to Dr. Robert Koeppel and Dr. Scott Snyder for their helpful comments.

References and notes

1. Fei, Y. J.; Ganapathy, V.; Leibach, F. H. *Prog. Nucl. Acid Res. Mol. Biol.* **1998**, *58*, 239.
2. Meredith, D.; Boyd, C. A. *Cell. Mol. Life Sci.* **2000**, *57*, 754.
3. Rubio-Aliaga, I.; Daniel, H. *Trends Pharmacol. Sci.* **2002**, *23*, 434.
4. Inui, K. I.; Masuda, S.; Saito, H. *Kidney Int.* **2000**, *58*, 944.
5. Herrera-Ruiz, D.; Knipp, G. T. *J. Pharm. Sci.* **2003**, *92*, 691.
6. Shen, H.; Smith, D.; Yang, T.; Huang, Y.; Schnermann, J.; Brosius, F. *Am. J. Physiol. Renal. Physiol.* **1999**, *276*, F658.
7. Smith, D. E.; Pavlova, A.; Berger, U. V.; Hediger, M. A.; Yang, T.; Huang, Y. G.; Schnermann, J. B. *Pharm. Res.* **1998**, *15*, 1244.
8. Shen, H.; Smith, D. E.; Keep, R. F.; Brosius, F. C., III. *Mol. Pharm.* **2004**, *1*, 248.
9. Döring, F.; Walter, J.; Will, J.; Föcking, M.; Boll, M.; Amasheh, S.; Clauss, W.; Daniel, H. *J. Clin. Invest.* **1998**, *101*, 2761.
10. Berger, U. V.; Hediger, M. A. *Anat. Embryol. (Berl)* **1999**, *199*, 439.
11. Groneberg, D.; Döring, F.; Nickolaus, M.; Daniel, H.; Fischer, A. *Neurosci. Lett.* **2001**, *304*, 181.
12. Nussberger, S.; Hediger, M. *Exper. Nephrol.* **1995**, *3*, 211.
13. Palacin, M.; Estevez, R.; Bertran, J.; Zorzano, A. *Physiol. Rev.* **1998**, *78*, 969.
14. Rubio-Aliaga, I.; Frey, I.; Boll, M.; Groneberg, D. A.; Eichinger, H. M.; Balling, R.; Daniel, H. *Mol. Cell Biol.* **2003**, *23*, 3247.
15. Shen, H.; Smith, D. E.; Keep, R. F.; Xiang, J.; Brosius, F. C., III. *J. Biol. Chem.* **2003**, *278*, 4786.
16. Tett, S. E.; Kirkpatrick, M. J.; Gross, A. S.; McLachlan, A. *J. Clin. Pharmacokinet.* **2003**, *42*(14), 1193.
17. Lam, Y. W.; Banerji, S.; Hatfield, C.; Talbert, R. L. *Clin. Pharmacokinet.* **1997**, *32*, 30.
18. Daniel, H.; Herget, M. *Am. J. Physiol.* **1997**, *273*, F1.
19. Adibi, S. A. *Ciba Found. Symp.* **1977**, *50*, 265.
20. Adibi, S. A.; Krzysik, B. A. *Clin. Sci. Mol. Med.* **1977**, *52*, 205.
21. Hidalgo, I. J.; Bhatnagar, P. L. C. P.; Miller, J.; Cucullino, G.; Smith, P. L. *Pharm. Res.* **1995**, *12*, 317.
22. Mizuma, T.; Masubuchi, S.; Awazu, S. *J. Pharm. Pharmacol.* **1998**, *50*, 167.
23. Terada, T.; Sawada, K.; Saito, M.; Hashimoto, Y.; Inui, K.-I. *Eur. J. Physiol.* **2000**, *440*, 679.
24. Wagner, J. G. *Fundamentals of Clinical Pharmacokinetics*; Drug Intelligence Publications: Hamilton, IL, 1975.
25. Daniel, H.; Morse, E. L.; Adibi, S. A. *J. Biol. Chem.* **1992**, *267*, 9565.
26. Goolcharran, C.; Borchardt, R. *J. Pharm. Sci.* **1998**, *87*, 283.
27. Purdie, J.; Benoiton, N. L. *J. Chem. Soc., Perkins Trans. 2* **1973**, 1845.
28. Capasso, S.; Mazzarella, L. *Peptides* **1998**, *19*, 389.
29. Sykes, B. D.; Robertson, E. B.; Dunford, H. B.; Konasewich, D. *Biochemistry* **1966**, *5*, 697.
30. The MMFF94 is one of the most reliable force fields for protein modeling in terms of predicting conformational energy differences and barrier height about single-bond torsions. See Refs. 31–33.
31. Levine, I. N. *Quantum Chemistry*, 5th ed.; Prentice Hall: Upper Saddle River, NJ, 1999, p 701.
32. Halgren, T. A.; Nachbar, R. B. *J. Comput. Chem.* **1996**, *17*, 587.
33. Halgren, T. A. *J. Comput. Chem.* **1999**, *20*, 720.
34. Calculations performed with the computational chemistry software package Spartan 02, release 116; Wavefunction, Inc.: Irvine, California.
35. Li, J. B. *J. Anal. Purif.* **1987**, *2*, 72.
36. Chase, B. H.; Downes, A. M. *J. Chem. Soc.* **1953**, 3874.
37. (a) Levene, P.; Bass, L.; Steiger, R. *J. Biol. Chem.* **1929**, *81*, 697; (b) Foye, W.; Kay, D. *J. Am. Pharm. Assoc.* **1960**, *49*, 705.
38. Harris, T.; Reilly, T.; DelPrincipe, J. *J. Heterocycl. Chem.* **1981**, *18*, 423.
39. Samaritoni, J. G.; Demeter, D. A.; Gifford, J. M.; Watson, G. B.; Kempe, M. S.; Bruce, T. J. *J. Agric. Food. Chem.* **2003**, *51*, 3035.
40. Jewett, D. *Appl. Radiat. Isot.* **1992**, *43*, 1383.
41. Slightly lower radiochemical yields were obtained when [^{11}C]methyl triflate was bubbled at ambient temperature.

42. Flow rate is 1.0 mL/min with Showa Denko polymethacrylate RSpak Shodex DE-613 (6.0 × 150 mm) HPLC column eluting at 5.1 min.
43. Sometimes it was necessary to reflux for longer than 8 min or use of 4 N NaOH to achieve total conversion when the solution volume remained over 1.5 mL.
44. Bai Ki, Q.; Holdsworth, C. H.; Asma, E.; Tai, Y. C.; Charziioannou, A.; Leahy, R. M. *Phys. Med. Biol.* **2002**, *47*, 2773.
45. Qi, J.; Leahy, R. M.; Cherry, S. R.; Charziioannou, A.; Furquhar, T. H. *Phys. Med. Biol.* **1998**, *43*, 1001.